



**Impact of confined geometries on hopping and trapping of motile bacteria in porous media**Lazaro J. Perez \**Division of Hydrologic Sciences, Desert Research Institute, Reno, Nevada 89512, USA*Tapomoy Bhattacharjee *The Andlinger Center for Energy and the Environment, Princeton University, Princeton, New Jersey 08544, USA*Sujit S. Datta *Department of Chemical and Biological Engineering, Princeton University, Princeton, New Jersey 08544, USA*Rishi Parashar  and Nicole L. Sund *Division of Hydrologic Sciences, Desert Research Institute, Reno, Nevada 89512, USA*

(Received 12 August 2020; accepted 4 January 2021; published 25 January 2021)

We use a random walk particle-tracking (RWPT) approach to elucidate the impact of porous media confinement and cell-cell interactions on bacterial transport. The model employs stochastic alternating motility states consisting of hopping movement and trapping reorientation. The stochastic motility patterns are defined based on direct visualization of individual trajectory data. We validate our model against experimental data, at single-cell resolution, of bacterial *E. coli* motion in three-dimensional confined porous media. Results show that the model is able to efficiently simulate the spreading dynamics of motile bacteria as it captures the impact of cell-cell interaction and pore confinement, which marks the transition to a late-time subdiffusive regime. Furthermore, the model is able to qualitatively reproduce the observed directional persistence. Our RWPT model constitutes a meshless simple method which is easy to implement and does not invoke *ad hoc* assumptions but represents the basis for a multiscale approach to the study of bacterial dispersal in porous systems.

DOI: [10.1103/PhysRevE.103.012611](https://doi.org/10.1103/PhysRevE.103.012611)**I. INTRODUCTION**

Bacterial migration through heterogeneous porous media is important for a wide range of processes, such as bioremediation, biofilm formation, and anticancer drug delivery [1–4]. In natural environments, bacteria employ diverse movement modalities while navigating through porous media that characterize their migration [5]. Motility is the capability of an organism to spontaneously perform independent moves, which enables bacteria to explore space and other resources and to forage or disperse. Bacterial transport, therefore, encapsulates processes that act across multiple spatial and temporal scales, which are key not only for innovative applications but also for their growth and interactions with the physical environment [6].

Many bacteria actively swim via flagella or twitch over surfaces. Disregarding the way they move, most observations of bacterial motility are undertaken in bulk fluid to avoid artifacts arising from surface and cell-cell interactions [7–9]. As a result, little is known about the effects that confined porous spaces have on motility. A common assumption is that bacteria perform linear short movements caused by collisions with the medium solid boundaries. Interaction between cells and cell-boundary collisions are thought to reorient cells,

similar to tumbles for *E. coli* [1] or flicks and reversals for *V. alginolyticus* [10], leading to a decreased diffusivity.

Traditionally, modeling the motility of many bacteria via flagella movement in aqueous systems has been conceptualized using two alternating movement periods due to the stochastic nature of bacterial motion [11,12]. Models assume that bacterial movement is composed of two modes: runs consisting of a linear straight movement followed by tumbles consisting of random changes in direction that mimic interaction between cells and collisions with obstacles [11,13–15]. Other methods may include particle-tracking techniques that rely on image segmentation algorithms [16], fitting cell's path curve to an evolving model [17], as well as non-Poissonian run-and-tumble patterns [18], suggesting that at least one of the steps in the regulation of reversal is thermodynamically irreversible.

Numerical observations assume that cell's movement is a stochastic process [10,11,19], and the derivation of its descriptive parameters requires clear discrimination of the stochastic patterns that relies on the rules that dictate random models. Random walk particle-tracking (RWPT) approaches have long been used to model cell migration [17,20,21]. Although this approach provides an expression for modeling cell migration, in most cases, the movement of individual cells cannot be attributed to a simple random walk behavior. Recent mathematical and modeling works have used modified random walk models by introducing repelling, reflecting, or absorbing

\*lazaro.perez@dri.edu

barriers, to account for bacterial interactions with solid boundaries and between cells [22–25]. Others intersperse two turning events in strictly alternating order to reproduce cell swimming directions. Despite some differences in the migration process modeled, these models commonly obviate transient short-time dynamics in motility states or how the diffusive dynamics depend on the run-and-tumble velocities and the switching probabilities between the two states.

A detailed mathematical analysis of the motility properties of microswimmers is essential for prediction of microbial dispersal under realistic conditions. Based on existing theories [26], we develop a two-state RWPT model that mimics and describes the hopping and trapping experimental dynamics reported in [27]. The model uses stochastic alternating motility states derived from direct inspection of cells' trajectory data. The model highlights the coupling between a cell's direction and its speed in confined geometries. We successfully capture the intermediate- and long-term spreading of *E. coli* in a confined porous medium.

The paper is organized as follows. Section II describes the experimental and data analysis methodology, as well as the RWPT approach. Section III discusses the motility patterns observed in the experimental visualization and presents the modeling results. Finally, we conclude and give an outlook on further expansion of our model in Sec. IV.

## II. METHODOLOGY

In the following, first we summarize the experimental setup presented by Bhattacharjee and Datta [27], whose data we use to evaluate our model's ability to reproduce the observed motility patterns. Then we recall the approach to analyze bacterial migration and discriminate between motility states. Finally, we present a numerical model to reproduce the observed findings in the experiment.

### A. Experimental data

As detailed in [27,28], we use confocal microscopy to visualize fluorescent *E. coli* (strain W3110) homogeneously dispersed in transparent, jammed packings of hydrogel particles. The packings act as solid matrices with macroscopic interparticle pores of average size  $\lambda = 1.9$  or  $3.6 \mu\text{m}$  that the cells can swim through. The internal mesh size of each hydrogel particle is much smaller than the individual cells but large enough to allow unimpeded transport of nutrients and oxygen, giving rise to homogeneous nutrient conditions throughout the packing.

In each experiment, we disperse the cells within 4 mL of a jammed hydrogel packing at  $6 \times 10^{-4}$  vol%, sufficiently dilute to minimize intercellular interactions, crossing of cellular trajectories, and any influence of nutrient consumption. We confine each medium inside a sealed glass-bottom petri dish, with a packing height of  $\sim 1$  cm, and add an overlying thin layer of  $750 \mu\text{L}$  liquid medium to prevent evaporation. We then use a Nikon A1R+ inverted laser-scanning confocal microscope with a temperature-controlled stage at  $30^\circ\text{C}$  to capture fluorescence images every 69 ms from an optical slice of  $79\text{-}\mu\text{m}$  thickness. The sampling interval of 69 ms is sufficiently fast to uniquely identify cells, since they do not move

more than approximately three cell body lengths between consecutive time points, while minimizing photobleaching of the fluorescent signal. Further, to avoid any boundary effects, all images are captured at least  $100 \mu\text{m}$  from the bottom of the container. Using this platform, we monitor bacterial motion through the pore space, acquiring projected two-dimensional movies within the porous media. To track the individual cells, we then use a custom MATLAB script developed in-house to identify and track each cell center using a peak finding function with subpixel precision using the classic Crocker-Grier algorithm [29]. We track cell motion for at least 10 s, five times longer than the unconfined run duration but over five times shorter than the cell division time, and focus our analysis on cells that exhibit motility within the tracking time.

This platform enabled us to discover a new mode of motility exhibited by *E. coli* in porous media [27]. Instead of moving via run-and-tumble dynamics with truncated runs, as is often assumed, we found that the cells are intermittently and transiently trapped in tight spots as they move through the pore space. When a cell is trapped, it constantly reorients its body until it is able to escape; it then moves in a directed path through the pore space, a process we call hopping, until it again encounters a trap.

### B. Trajectory analysis

In order to perform behavior discrimination, several quantitative features have been proposed such as the average velocity [1], moving average of incremental displacements (MAID) [15], and turning events [30,31]. Here, we use the MAID to distinguish between motility states in the extracted bacterial trajectories from [27]. The MAID has performed well in discriminating hopping and trapping modes compared to other features in a limited number of bacterial trajectories [15].

Differences in bacterial motility modes lead to significant effects on their migration. For instance, bacterial trapping produces a significant decrease in the effective swimming speed, and thus a decrease in incremental displacement is expected. By contrast, the incremental displacements during the hopping mode increases [1,15]. Therefore, incremental displacements, defined as the Euclidean distance between two consecutive points in a cell trajectory, can be used quantitatively to discriminate between hopping and trapping states. In our case, hopping and trapping states were identified by means of bacterial speed as the threshold parameter before the MAID was applied. The moving average of the incremental displacements reduces noise effects in the incremental displacements analysis given as

$$\kappa_t = \frac{1}{w} \sum_{i=-(w-1)/2}^{(w-1)/2} d_{t+i}, \quad (1)$$

where  $w$  is the window size for calculating the moving average of the incremental distance  $\kappa$  at time  $t$ , and  $d_{t+i}$  is the Euclidean distance between consecutive time steps in a cell trajectory. We extract the motility parameters that govern bacterial transport separately for the hopping and trapping modes to characterize our mathematical model. In summary, when a cell speed is above the ensemble trajectory average speed, the

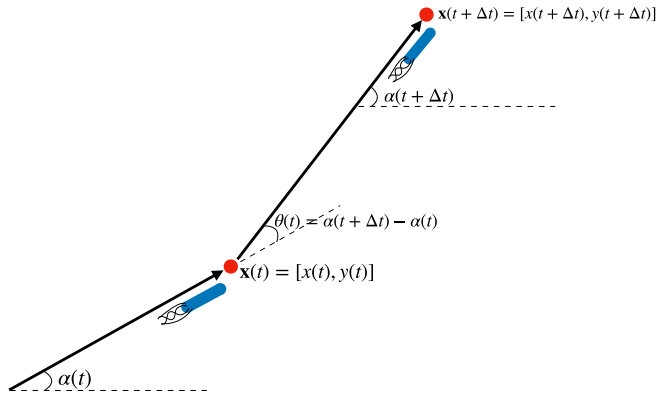


FIG. 1. Illustration of the trajectory of a cell during two successive steps.

cell is considered to be in a hop. On the other hand, if the cell speed is below the ensemble trajectory average speed, the cell is regarded to be in a trapping state. We chose this specific parameter value because it provides a good comparison between the obtained classification of hopping and trapping and the traditional runs and tumbles [15,31–33]. We performed a sensitivity analysis of other criteria to discriminate between motility states (e.g., deviation angle variance) and the resulting statistical characteristics of the analyzed trajectories were robust to variations as large as  $\sim 10\%$ . We determined the marginal distribution of velocities for the hopping and trapping modes from the trajectory analysis [15] to analyze and understand the pore-scale cell motion, which constitutes a central part in the developed model. The change in the trajectory direction or body orientation,  $\theta$ , with respect to the arrival direction in a given time step is computed from the bearing angle  $\alpha$  from  $\mathbf{x}(t)$  to  $\mathbf{x}(t + \Delta t)$  as the angle measured in the clockwise direction from the line segment to the horizontal line,

$$\tan \alpha(t) = \frac{y(t + \Delta t) - y(t)}{x(t + \Delta t) - x(t)}, \quad (2)$$

where  $\mathbf{x}(t) = [x(t), y(t)]$  is the position of the cell at time  $t$  and  $\Delta t$  is the experimental sampling interval. Figure 1 shows the trajectory of a cell during two successive steps and how we extract  $\alpha$  and  $\theta$  from the pathways of each cell obtained from the particle-tracking module.

Our emphasis is on the comparison between simulations and experimental data, therefore we assess the accuracy of our numerical model based on the computed mean squared displacement (MSD), given as

$$\text{MSD}(\mathcal{S}) = \langle |\mathbf{x}(t + \mathcal{S}) - \mathbf{x}(t)|^2 \rangle, \quad (3)$$

where  $|\mathbf{x}(t + \mathcal{S}) - \mathbf{x}(t)|$  is the particle displacement between two time points,  $t$  denotes the absolute time, and  $\mathcal{S}$  is the so-called lag time [1]. Additional information about the experimentally observed bacterial behavior can be extracted from the normalized velocity autocorrelation function  $C$ ,

$$C(\mathcal{S}) = \frac{\langle \mathbf{v}(t + \mathcal{S}) \cdot \mathbf{v}(t) \rangle}{\langle v^2(t) \rangle}, \quad (4)$$

where  $\mathbf{v}$  stands for the velocity.  $C$  can also be found by double differentiation of the MSD.

### C. Mathematical model

To describe quantitatively the dispersal dynamics that bacteria exhibit in [27], we propose the random walk model

$$\mathbf{x}(t + \Delta t) = \mathbf{x}(t) + \mathbf{v}_m(t)\Delta t + \sqrt{2D\Delta t}\boldsymbol{\xi}(t), \quad (5)$$

where  $\mathbf{v}_m$  is the motile velocity vector, and the diffusion coefficient  $D$  is approximated from the experimental data as

$$D = \frac{\langle [\mathbf{x}(t_m) - \mathbf{x}(t_m - \mathcal{S})]^2 \rangle}{6t_m}, \quad (6)$$

where  $t_m$  is the maximum observation time.  $D$  varies from  $0.53 \mu\text{m}^2/\text{s}$  for  $\lambda = 1.9 \mu\text{m}$  to  $5.71 \mu\text{m}^2/\text{s}$  for  $\lambda = 3.6 \mu\text{m}$ . We substitute a shifted and scaled uniform  $[0, 1]$  random variable  $\sqrt{24D\Delta t}(\mathbf{U}(0, 1) - 1/2)$  for the last term, where  $\mathbf{U}(0, 1)$  is a vector of independent and identically distributed uniform random variables between 0 and 1 [34,35]. This choice avoids the costly numerical generation of Gaussian random numbers. The central limit theorem guarantees that the sum of random displacements is again Gaussian. Each particle represents a single cell that moves at velocity  $\mathbf{v}_m(t) \sim v_m(t)\mathbf{e}(t)$ , where the subscript  $m$  stands for the motility mode. The speed  $v_m(t)$  is the velocity of the cell and the unit vector  $\mathbf{e}(t)$  denotes the direction of propagation at time  $t$ . The velocity magnitude and direction are simulated according to

$$\mathbf{v}_m(t) = v_m(t) \begin{pmatrix} \cos(\theta_m(t)) \\ \sin(\theta_m(t)) \end{pmatrix}, \quad (7)$$

where  $\theta_m(t)$  is randomly chosen according to the turning-angle distribution  $p_h(\theta)$  or  $p_t(\theta)$  in the hopping or trapping state, respectively. While the speed  $v_m(t)$  is chosen from a marginal velocity distribution that depends on the  $\theta$  chosen in each motility mode. This  $v_m(t)$  selection preserves the correlation between  $\theta$  and  $v_m$  extracted from the trajectory analysis. We use the methodology presented in [36,37] as the sampling method to select  $\theta_m$  and  $v_m$  from their known distributions.

The transitions between the motility states are determined based on the probability distributions obtained from the observed experimental trajectories. We found that the observed duration distribution of staying in the hopping state is well fitted by an exponential distribution; moreover, while the observed duration distribution of staying in the trapping state shows a long nonexponential tail, an exponential distribution provides a reasonable approximation for our computations. These findings have been observed in other *E. coli* experiments [5,33,38]. In our case, hopping times are approximated to be exponentially distributed with a mean hopping time  $\tau_h$ , thus we use a hopping transition probability of the form

$$P(t < t + \Delta t) \sim e^{-(t-t_0)/\tau_h}, \quad (8)$$

where  $t - t_0$  is the time passed since the previous change of state. Equation (8) describes the hopping probability; the trapping transition probability is analogous. Note that the probability of starting the motion in the hop or trap phase is denoted  $P_0^h$  and  $P_0^t$ , respectively, with

$$P_0^t = 1 - P_0^h. \quad (9)$$

The choice of an initial fixed hop probability [39] for all the particles showed no significant impact on the results here.

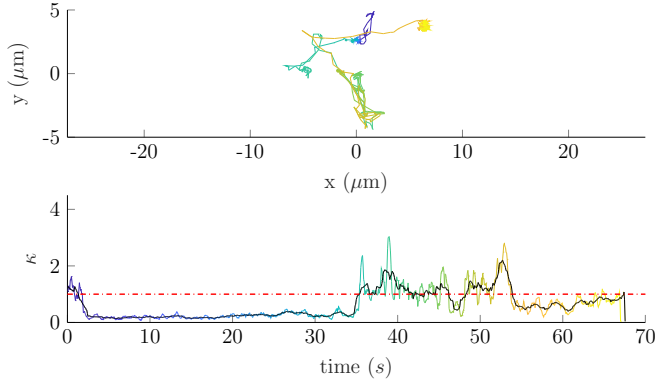


FIG. 2. Top: Trajectory of one cell. Bottom: Normalized MAID in which the color-coded line shows the initial position (blue) and final position (yellow) in the cell trajectory. The dashed-dotted red line delineates hopping from the trapping mode. The solid black line corresponds to the MAID with a higher value of  $w$ .

The occurrence of a motility mode transition event is determined through a Bernoulli trial based on the transition probability, (8).

In our numerical setup, the bacterial transport problem is solved with the RWPT simulator described, (5). As the initial condition for simulations of both pore length experiments analyzed, we consider uniform areal distributions of particles from  $[10, 120] \mu\text{m}$  and  $[5, 70] \mu\text{m}$ , in  $x$  and  $y$  coordinates, respectively. We implement bacterial confinement and collective dynamics assuming physical interaction between swimmers. When a particle is in the hopping mode and closer than a cell body length,  $\gamma = 2 \mu\text{m}$ , to another particle, its motility mode changes to the trapping mode with  $P = 1$ , as a result of the collision [21,24,33,40].

### III. RESULTS

In the following, we study the transport dynamics of the experimental analysis in terms of the hopping and trapping discrimination for bacterial motility states. First, we describe the motility patterns for the evaluated bacterial states observed in the experimental visualization, which are the building blocks of the mathematical model presented in the previous section.

#### A. Motility patterns

We analyzed 41 cell trajectories with an average length of 12.42 s following the procedure detailed in the previous section. A typical trajectory is shown in Fig. 2 (upper plot), with the starting and final points, respectively, indicated by blue and yellow marks. The corresponding color-coded MAID plot versus time in Fig. 2 (lower plot) shows hopping and trapping discrimination based on the normalized ensemble mean incremental displacement or, in other words, the cells' ensemble mean velocity. Segments below 1 are identified as trapping states, while segments above the normalized threshold indicate that the cells are in the hopping mode. As for window sizes in MAID features,  $w$  values of 5 to 21 were tested to illustrate the impact of the  $w$  value in the results to avoid artificial smoothing from higher  $w$  values. Results

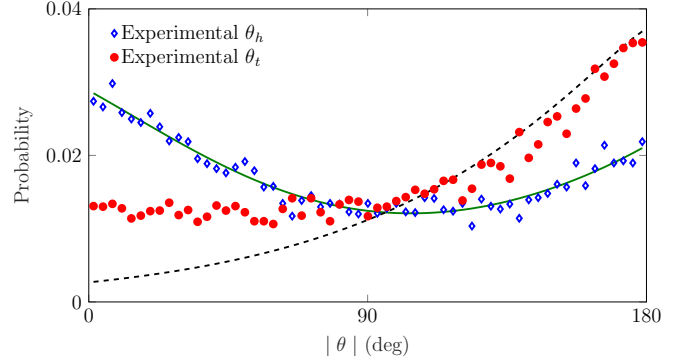


FIG. 3. Turn-angle distributions of the hopping (blue diamonds) and trapping (red circles) mode from the smallest pore size ( $1.9 \mu\text{m}$ ) in the experimental data and their fitted distributions (solid and dashed lines).

of this analysis show that  $w = 9$  provides the best result in differentiating the hopping and trapping modes. Nonetheless, a window size of 21 (solid black line in Fig. 2, lower plot), which implies a higher smoothing degree, provides optimal results in reducing noise without losing relevant information for bacterial motility state discrimination. The methodology, thus, mitigates the error propagation in the evaluation of the state discrimination in noisy data by optimizing bacterial motility data and avoiding visual calibrated motility state discrimination [33] from the empirical data.

Classical bacterial transport models fitted bacteria orientation angles undergoing run-and-tumble cycles using uniform distributions [41]. Experimentally, this means that, when a cell swims around rounded obstacles over a long enough time, the probability density function of  $\theta$  should be uniform, as it eventually samples all values of the cell body orientation angle ( $\theta$ ) within the plane of that surface with equal probability. This is also true for the overall orientation angles of an entire population of bacteria, as long as the cell trajectories are independent and interactions between trajectories (such as cell collisions or hydrodynamic interactions) are random with no long-range correlations or event memory. This traditional notion changes in the presence of chemical gradients, medium confinement, or flow [15,27,31,42]. The results of the  $\theta$  orientation angle distribution from the experimental  $\lambda = 1.9 \mu\text{m}$  shown in Fig. 3 suggest straight hops and reverse turns in the trapping mode, which is consistent with the run-reverse concept due to flagellar rotation [5,43]. We observe that the key difference between hopping and trapping is the ability of the cell to maintain its direction of motion during the course of a hop, while when trapped, the cell reverses its orientation, which allows bacteria to escape bead traps by reversing their swim [43–45]. This feature sheds lights on the classical notion that broadly distributed angles for the trapping mode indicate that their motion is uniform randomly oriented. Therefore, angular distributions in different motility modes cannot be ignored, as they provide information on bacterial swimming strategy. The turn-angle distribution for both modes is bimodal, with higher peaks near lower and higher values of  $|\theta|$ . The distribution parameters,  $\mu_h = [0.02\pi, 0.88\pi]$  and  $\mu_t = [-0.94\pi, 0.89\pi]$ , while  $\sigma_h$  and  $\sigma_t$  are  $[0.69, 0.94]$  and



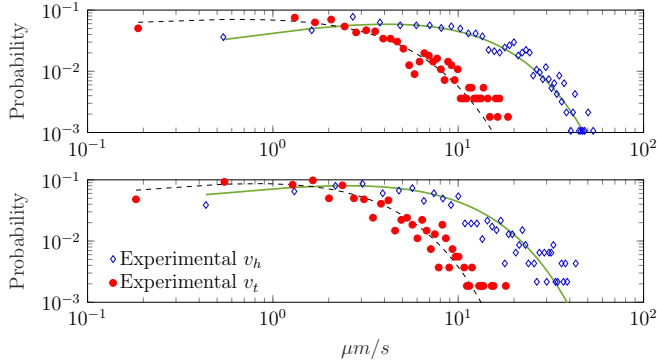


FIG. 4. Marginal velocity distribution for hopping (blue squares) and trapping (red circles) states from the smallest pore size ( $\lambda = 1.9 \mu\text{m}$ ) in the experimental data and their fitted gamma distribution (solid and dashed lines, respectively) for  $|\theta| = [0, 10]$  (upper plot) and  $|\theta| = [60, 70]$  (lower plot).

[0.85, 0.85], respectively, were found by fitting a Gaussian mixture model to the data [46]. The bimodal distribution in turn-angle distributions indicates that when a cell chooses a new direction, it is most likely to choose a new direction not very different from or opposite to the previous direction. This distribution is qualitatively similar to the reported for *E. coli* strains AW405 [47] and O157:H7 [48] and for *Pseudomonas putida* [49,50]. We find similar behavior for  $\lambda = 3.6 \mu\text{m}$ , thus we omit these data here and focus on the small pore size case.

Figure 4 shows the marginal velocity distributions from experimental data for  $\lambda = 1.9 \mu\text{m}$  for two  $|\theta|$  ranges. We found that the gamma distribution is the continuous distribution that best fit the experimental marginal velocity distributions for the hopping and trapping modes (Fig. 4). The gamma-fitted distribution shows a smaller root mean square error than other continuous distributions (log-normal, beta, generalized extreme value) that were tested. This result is the one expected for motile bacteria and suggests signs of enhanced transport processes over a scale larger than the pore size [15,51]. It can be observed in Fig. 4 that, as expected, the hopping state marginal distribution is slightly shifted to higher values for lower  $|\theta|$  ranges and thus shows a higher mean velocity,  $\bar{v}_{h,|\theta|=[0,10]} = 12.33 \mu\text{m/s}$  (Fig. 4, upper plot) than for higher  $|\theta|$  ranges, where  $\bar{v}_{h,|\theta|=[60,70]} = 9.16 \mu\text{m/s}$  (Fig. 4, lower plot). The overall mean velocity for the hopping state is  $\bar{v}_h = 9.26 \mu\text{m/s}$ . The  $k$  and  $\beta$  parameters for the fitted gamma distributions for the hopping state showed variations such as  $1.31 < k < 1.77$  and  $4.01 < \beta < 8.54$ . The trapping state marginal distributions display small variations for the different  $|\theta|$  ranges, showing the highest,  $\bar{v}_t = 3.87 \mu\text{m/s}$  ( $k = 1.12$  and  $\beta = 3.53$ ), for  $|\theta| = [10, 20]$  and the lowest,  $\bar{v}_t = 2.95 \mu\text{m/s}$  ( $k = 1.42$  and  $\beta = 2.14$ ), for  $|\theta| = [120, 130]$ , with an overall  $\bar{v}_t = 3.22 \mu\text{m/s}$ .

The distributions of hop and trapping times are shown in Fig. 5, where both modes are well fit by exponential distributions. Note that while there is some deviation in the tail of the trapping distribution (consistent with a power law [28]), the exponential fit provides a good first approximation. The mean hop time  $\tau_h$  is given by the average value of the experimentally derived hop times,  $\tau_h = 0.926 \text{ s}$  for  $\lambda = 1.9 \mu\text{m}$  and  $\tau_h = 0.804 \text{ s}$  for  $\lambda = 3.6 \mu\text{m}$ . The lower value of  $\tau_h$  for the greatest

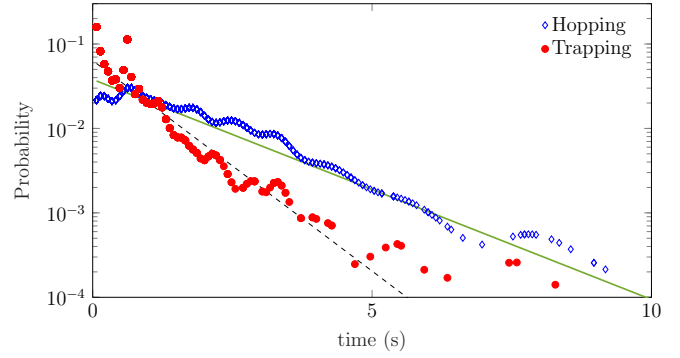


FIG. 5. Experimental distribution of the duration of staying in the hopping (blue diamonds) and trapping (red circles) modes and best-fitting exponential distributions (solid green and dashed black lines).

$\lambda$  is attributed to higher frequencies of short hops [31]. On the other hand, the mean trapping time  $\tau_t$  for  $\lambda = 1.9$  and  $\lambda = 3.6 \mu\text{m}$  are 0.44 and 0.42 s, respectively. The exponential distribution is a simplifying assumption, which is, however, crucial for the modeling calculations.

### B. Model comparison to experimental results

Based on the information extracted from the trajectory analysis, we simulate 5000 bacterial trajectories in the absence of chemotaxis using the random walk algorithm presented above. We validate the model against the experimental results [27].

Results of the computed velocity autocorrelation from the simulation and experimental data are shown in Fig. 6. Time is made dimensionless by considering  $t' = t/\tau_h$ . For simplicity of notation, we omit the primes in the following. We find that the RWPT model provides a good description of the experimental velocity autocorrelation function. In particular, the model captures the shape of the experimental velocity autocorrelation function including the reproduction of the negative dip. This further justifies that the RWPT model used is appropriate to describe the motility patterns of *E. coli* in a confined geometry. We hypothesize that the quick decay and negative peak observed in *C* are due to pore confinement. This

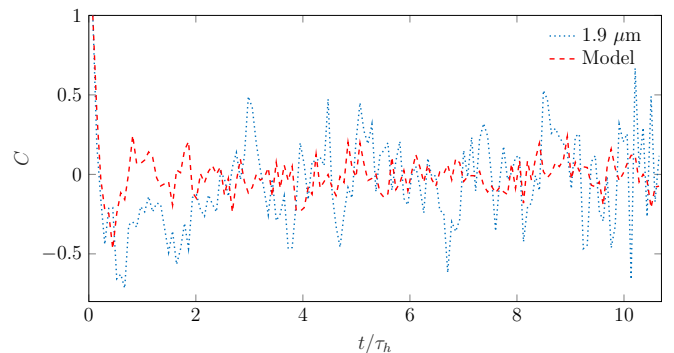


FIG. 6. Normalized experimental (dotted blue line) and model (dashed red line) velocity autocorrelation function plotted as a function of the dimensionless time  $t/\tau_h$ .

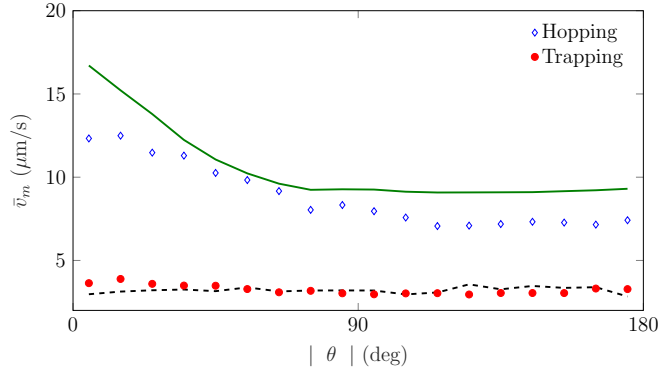


FIG. 7. Bacterial directional persistence in terms of different turning-angle ranges at  $\lambda = 1.9 \mu\text{m}$  for the hopping and trapping modes. Experimental and modeling results are represented by symbols and lines, respectively.

observation is supported by direct inspection of individual trajectory data. A clear example of this is inferred from the lower plot in Fig. 2, where the plot of  $\kappa$  shows that the cell starts in the hopping mode but changes its motility mode to trapping at  $t < \tau_h$ . Traditionally, this behavior in  $C$  has been described as the preconfined regime in RWPT models in confined geometries [21,52,53].

We now discuss the model's ability to reproduce bacterial directional persistence to determine whether turning angle ranges of the bacterial population affect the observed speed. We split up our data set of 10 356 hopping and 13 086 trapping speeds for  $\lambda = 1.9 \mu\text{m}$  to create separate velocity distributions for 18 different turning-angle ranges. Please note that for our simulation model we fit the gamma distribution as explained in the previous section to the velocities distributions. Figure 7 shows the mean instant velocity of each motility mode for different  $|\theta|$  ranges. We find directional persistence in experimental data in the hopping mode, as results indicate that turning-angle ranges  $[0, 10)$  and  $[10, 20)$  show higher mean velocities than the rest of the  $|\theta|$  ranges. These results support the idea that higher velocities correspond to straight hops [27,47] and, thus, coupling between  $v_h$  and  $|\theta|$ . At higher  $|\theta|$  range intervals, we observe a decrease in mean velocities in hops, which indicates that when cells perform high-angle turns in the hopping mode they reduce their instant velocity and that hops after cell reorientation are smaller than the bacterial population mean. The model shows higher average swimming speeds ( $\bar{v}_m$ ) in the hopping mode. The discrepancy between experimental and model observations is attributed to a broader swimming speed sampling around the mean in the experimental observations. Note that model results for hopping approach the reported experimental  $\bar{v}_h$  after  $\bar{\theta}_h$ . On the other hand, Fig. 7 shows that the trapping mode exhibits a more stable range of mean instant velocities around the reported  $\bar{v}_t$ . We find good agreement between model and experimental evidence. Our findings shed light on the mechanisms underlying cell reorientation as *E. coli* swimming is driven by the rotation of flagella. The resulting reorientation is commonly modeled using rotational diffusion, which implies a persistence that decreases exponentially with the trapping duration [30,32] that fails to capture bacterial

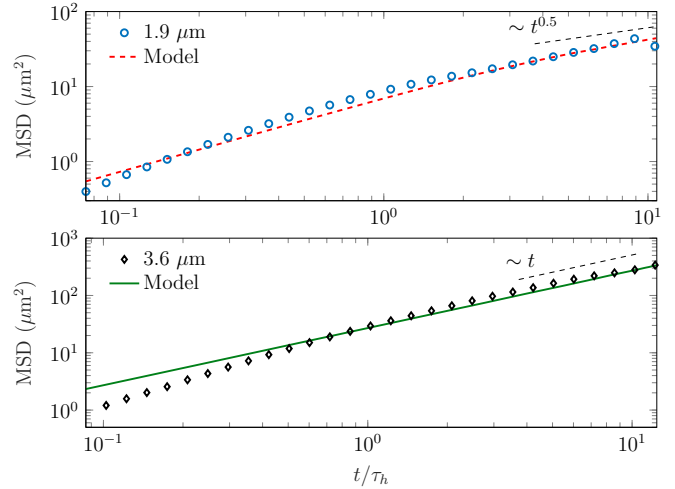


FIG. 8. Evolution of the mean squared displacement (MSD) computed for different pore sizes,  $1.9 \mu\text{m}$  (upper plot) and  $3.6 \mu\text{m}$  (lower plot). The experimental MSD is represented by symbols in both plots, and the RWPT simulation results for  $1.9 \mu\text{m}$  (dashed red line in upper plot) and  $3.6 \mu\text{m}$  (solid green line in lower plot).

dispersion at late times. Moreover, the changes in mean instant velocities according to  $|\theta|$  that we observe do not result from differences in trapping duration. Further imaging studies of swimming cells with labeled flagella may be able to clarify this observation.

Results of the computed MSD from both the experimental and the simulated trajectories are presented in Fig. 8. At early times, we observe that the experimental MSD for both pore length experiments,  $t \ll \tau_h$ , shows a superdiffusive regime which our model is not able to capture as the MSD from simulations exhibits diffusive behavior at early times. The discrepancy between model and experiment can be attributed to the use of the approximated  $D$  coefficient following (6) in the diffusive step in (5), which does not quantify proper spreading at  $t \ll \tau_h$ . As  $t$  approaches  $\tau_h$ , a transition to a diffusive regime occurs. The transition happens because cell-cell and cell-obstacle interaction effects increase, which affects bacterial step lengths and, thus, their motility behavior. Please note that the duration of superdiffusive motion decreases as pore confinement increases (Fig. 8). This is observed by direct comparison of the experimental MSDs for the two pore sizes, which reveals that the superdiffusive behavior at  $\lambda = 3.6 \mu\text{m}$  (Fig. 8, lower plot) and  $\lambda = 1.9 \mu\text{m}$  (Fig. 8, upper plot) lasts  $t = 0.5\tau_h$  and  $t = 0.15\tau_h$ , respectively. There is good agreement between experimental and model results. At late times, the emergence of a subdiffusive regime is observed in the case of  $\lambda = 1.9 \mu\text{m}$ , where bacterial confinement leads to nonlinear behavior, which is consistent with previous observations [54]. This subdiffusive phenomenon is delayed in the larger pore size but is also expected for  $t \gg 10$ . Note that we restricted our experimental analysis to 10 s because of noisy data at longer times. The late-time subdiffusive regime is reflected in the evolution of the experimental MSD, which increases as  $\sim t^{1/2}$ , shown in Fig. 8 (upper plot). The nonlinear increase in the MSD is well described by the RWPT model, as it captures interaction between cells and pore confinement,

which affects bacterial motility. In addition, the late-time agreement between model and experimental data in Fig. 8 (upper plot) stems from the correct characterization of the experimental directional persistence in the trapping mode as subdiffusive dynamics are commonly attributed to trapping states [54,55]. Analysis of the MSD of individual cells for  $\lambda = 1.9 \mu\text{m}$  reveals that subdiffusive behavior may be transient and collapses back to normal diffusion in some cells. This effect is masked in averaging. The transient subdiffusive behavior has been observed in experimental cases of obstructed diffusion [56] and computational models [25] at sufficiently long times. We remark that our analysis is limited due to the finite-size effect at long times, thus we do not observe such transient behavior in the global MSD. A detailed analysis of this limitation is discussed in the Appendix.

The RWPT model presented here is able to accurately model bacterial transport in confined porous media in an effective way. Our RWPT model differs from previous modeling attempts using two transport modes, which neglect the angular distribution in the trapping mode and use only the two preferred turning angles in this mode to model cell transport [5,31]. Most importantly, our proposed approach provides a means to define a quantitative measure to understand the transition spectrum between the hopping and the trapping modes and its impact on different variations of trajectory.

#### IV. CONCLUSIONS

We use pattern recognition techniques in a direct visualization of bacterial migration to extract statistical parameters used as input for the trajectory simulations. The analysis of turn-angle distributions in combination with speed shows coupling, which suggests directional persistence in bacterial trajectories. This means that when cells are moving fast the probability of staying on a directed path through the pore space is high. Moreover, when cells encounter a trap they reorient its body until it is able to escape with an almost-uniform distribution of speed. Inspection of the transport dynamics shows that for both hopping and trapping modes, the gamma distribution fits the marginal velocity best, while an exponential distribution shows that it describes well the hopping and trapping-time distributions when used as an approximation. These observations thus contradict the paradigm of run-and-tumble motility which traditionally is assumed to persist in a porous medium [1] and clarifies the impact of porous medium confinement on bacterial motility.

Our RWPT model describes well the transport dynamics of motile bacteria observed in the experimental visualization analyzed, as it takes into account the constraints imposed by the device itself and its obstacles, as well as cell-cell collisions, which may induce the subdiffusive behavior observed in the smaller pore size. Moreover, the model provides a good description of the observed MSD and velocity autocorrelation functions. This is further justification that the RWPT approach is appropriate to describe the motility patterns of *E. coli* in confined porous media. The approach used imposes no statistical restrictions on the stochastic processes representing bacterial spatial random increments. Each particle moves based on alternating motility states based on the information extracted from the trajectory analysis and Brownian diffusion.

The RWPT framework used can also provide a systematic approach to extract knowledge of and insights into bacterial motility that leads to a better understanding of bacterial behavior at larger scales.

#### ACKNOWLEDGMENTS

The work of L.J.P., R.P., and N.L.S. was financially supported by US Department of Energy (DOE) Grant No. DE-SC0019437. L.J.P. acknowledges the support of the Desert Research Institute (DRI) through Post Doc Support (PG19123). Work by T.B. and S.S.D. was supported by NSF Grant No. CBET-1941716, the Project X Innovation Fund, a distinguished postdoctoral fellowship from the Andlinger Center for Energy and the Environment at Princeton University to T.B., and, in part, funding from the Princeton Center for Complex Materials, a Materials Research Science and Engineering Center supported by NSF Grant No. DMR-2011750.

#### APPENDIX: FINITE-SIZE EFFECTS ON EXPERIMENTAL DATA

We illustrate here the full evolution of the experimental global MSD (Fig. 9), which suggests that a late diffusive regime arises after the subdiffusive behavior. However, at these long times where the transition is expected to occur, we lost  $\sim 30\%$  of the cells tracked at  $\lambda = 1.9 \mu\text{m}$  and  $\sim 25\%$  at  $\lambda = 3.6 \mu\text{m}$ ; such data reduction affects the MSD observed, and consequently noisy data appear. This limitation prevents us from claiming that the subdiffusive behavior is transient and collapses back to normal diffusion. On the other hand, the model captures such subdiffusion transiency and predicts a diffusive regime at  $t \gg \tau_h$ , however, the crossover time at which our RWPT converges to the diffusive behavior cannot be verified against our experimental data.

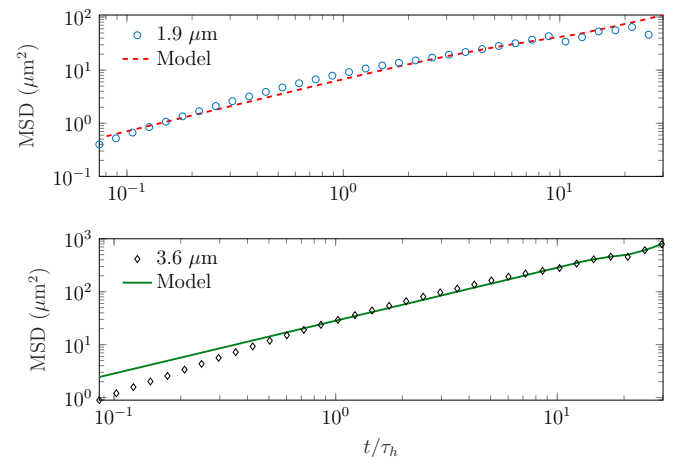


FIG. 9. Full evolution of the mean squared displacement (MSD) computed for different pore sizes,  $1.9 \mu\text{m}$  (upper plot) and  $3.6 \mu\text{m}$  (lower plot). The experimental MSD is represented by symbols in both plots, and the RWPT simulation results for  $1.9 \mu\text{m}$  (dashed red line in upper plot) and  $3.6 \mu\text{m}$  (solid green line in lower plot).

- [1] P. S. Lovely and F. Dahlquist, Statistical measures of bacterial motility and chemotaxis, *J. Theor. Biol.* **50**, 477 (1975).
- [2] R. Singh, D. Paul, and R. K. Jain, Biofilms: Implications in bioremediation, *Trends Microbiol.* **14**, 389 (2006).
- [3] S. J. Edwards and B. V. Kjellerup, Applications of biofilms in bioremediation and biotransformation of persistent organic pollutants, pharmaceuticals/personal care products, and heavy metals, *Appl. Microbiol. Biotechnol.* **97**, 9909 (2013).
- [4] J. Song, Y. Zhang, C. Zhang, X. Du, Z. Guo, Y. Kuang, Y. Wang, P. Wu, K. Zou, L. Zou *et al.*, A microfluidic device for studying chemotaxis mechanism of bacterial cancer targeting, *Sci. Rep.* **8**, 6394 (2018).
- [5] J. Taktikos, H. Stark, and V. Zaburdaev, How the motility pattern of bacteria affects their dispersal and chemotaxis, *PLoS One* **9**, e92348 (2013).
- [6] D. Scheidweiler, F. Miele, H. Peter, T. J. Battin, and P. de Anna, Trait-specific dispersal of bacteria in heterogeneous porous environments: From pore to porous medium scale, *J. R. Soc. Interface* **17**, 20200046 (2020).
- [7] P. D. Frymier, R. M. Ford, H. C. Berg, and P. T. Cummings, Three-dimensional tracking of motile bacteria near a solid planar surface, *Proc. Natl. Acad. Sci. U.S.A.* **92**, 6195 (1995).
- [8] G. Li, L.-K. Tam, and J. X. Tang, Amplified effect of Brownian motion in bacterial near-surface swimming, *Proc. Natl. Acad. Sci. U.S.A.* **105**, 18355 (2008).
- [9] X. Yang, R. Parashar, N. L. Sund, A. E. Plymale, T. D. Scheibe, D. Hu, and R. T. Kelly, On modeling ensemble transport of metal reducing motile bacteria, *Sci. Rep.* **9**, 14638 (2019).
- [10] L. Xie, T. Altindal, S. Chattopadhyay, and X.-L. Wu, Bacterial flagellum as a propeller and as a rudder for efficient chemotaxis, *Proc. Natl. Acad. Sci. U.S.A.* **108**, 2246 (2011).
- [11] V. Arabagi, B. Behkam, E. Cheung, and M. Sitti, Modeling of stochastic motion of bacteria propelled spherical microbeads, *J. Appl. Phys.* **109**, 114702 (2011).
- [12] C. E. López, A. Théry, and E. Lauga, A stochastic model for bacteria-driven micro-swimmers, *Soft matter* **15**, 2605 (2019).
- [13] N. A. Licata, B. Mohari, C. Fuqua, and S. Setayeshgar, Diffusion of bacterial cells in porous media, *Biophys. J.* **110**, 247 (2016).
- [14] F. Detcheverry, Generalized run-and-turn motions: From bacteria to Lévy walks, *Phys. Rev. E* **96**, 012415 (2017).
- [15] X. Liang, N. Lu, L.-C. Chang, T. H. Nguyen, and A. Massoudieh, Evaluation of bacterial run and tumble motility parameters through trajectory analysis, *J. Contam. Hydrol.* **211**, 26 (2018).
- [16] G. Danuser, J. Allard, and A. Mogilner, Mathematical modeling of eukaryotic cell migration: Insights beyond experiments, *Annu. Rev. Cell Dev. Biol.* **29**, 501 (2013).
- [17] R. S. Marken and W. T. Powers, Random-walk chemotaxis: Trial and error as a control process, *Behav. Neurosci.* **103**, 1348 (1989).
- [18] L. Xie, T. Altindal, and X.-L. Wu, An element of determinism in a stochastic flagellar motor switch, *PLoS One* **10**, e0141654 (2015).
- [19] F. Safaeifard, S. P. Shariatpanahi, and B. Goliaei, A survey on random walk-based stochastic modeling in eukaryotic cell migration with emphasis on its application in cancer, *Multidisciplin. Cancer Invest.* **2**, 1 (2018).
- [20] W. Alt, Biased random walk models for chemotaxis and related diffusion approximations, *J. Math. Biol.* **9**, 147 (1980).
- [21] H. Karani, G. E. Pradillo, and P. M. Vlahovska, Tuning the Random Walk of Active Colloids: From Individual Run-and-Tumble to Dynamic Clustering, *Phys. Rev. Lett.* **123**, 208002 (2019).
- [22] R. Parashar, D. O'Malley, and J. H. Cushman, Mean first-passage time for superdiffusion in a slit pore with sticky boundaries, *Phys. Rev. E* **78**, 052101 (2008).
- [23] R. Parashar and J. H. Cushman, Scaling the fractional advective-dispersive equation for numerical evaluation of microbial dynamics in confined geometries with sticky boundaries, *J. Comput. Phys.* **227**, 6598 (2008).
- [24] T. Marquez-Lago, A. Leier, and K. Burrage, Anomalous diffusion and multifractional Brownian motion: Simulating molecular crowding and physical obstacles in systems biology, *IET Syst. Biol.* **6**, 134 (2012).
- [25] F. Höfling and T. Franosch, Anomalous transport in the crowded world of biological cells, *Rep. Prog. Phys.* **76**, 046602 (2013).
- [26] B. ten Hagen, S. van Teeffelen, and H. Löwen, Brownian motion of a self-propelled particle, *J. Phys.: Condens. Matter* **23**, 194119 (2011).
- [27] T. Bhattacharjee and S. S. Datta, Bacterial hopping and trapping in porous media, *Nat. Commun.* **10**, 2075 (2019).
- [28] T. Bhattacharjee and S. S. Datta, Confinement and activity regulate bacterial motion in porous media, *Soft Matter* **15**, 9920 (2019).
- [29] J. C. Crocker and D. G. Grier, Methods of digital video microscopy for colloidal studies, *J. Colloid Interface Sci.* **179**, 298 (1996).
- [30] M. Theves, J. Taktikos, V. Zaburdaev, H. Stark, and C. Beta, A bacterial swimmer with two alternating speeds of propagation, *Biophys. J.* **105**, 1915 (2013).
- [31] E. V. Pankratova, A. I. Kalyakulina, M. I. Krivososov, S. V. Denisov, K. M. Taute, and V. Y. Zaburdaev, Chemotactic drift speed for bacterial motility pattern with two alternating turning events, *PLoS One* **13**, e0190434 (2018).
- [32] J. Taktikos, V. Zaburdaev, and H. Stark, Modeling a self-propelled autochemotactic walker, *Phys. Rev. E* **84**, 041924 (2011).
- [33] J. E. Sosa-Hernández, M. Santillán, and J. Santana-Solano, Motility of *Escherichia coli* in a quasi-two-dimensional porous medium, *Phys. Rev. E* **95**, 032404 (2017).
- [34] L. J. Perez, J. J. Hidalgo, and M. Dentz, Reactive random walk particle tracking and its equivalence with the advection-diffusion-reaction equation, *Water Resour. Res.* **55**, 847 (2019).
- [35] A. Puyguiraud, L. J. Perez, J. J. Hidalgo, and M. Dentz, Effective dispersion coefficients for the upscaling of pore-scale mixing and reaction, *Adv. Water Resour.* **146**, 103782 (2020).
- [36] G. Marsaglia and W. W. Tsang, A simple method for generating gamma variables, *ACM Trans. Math. Softw.* **26**, 363 (2000).
- [37] L. Martino and J. Míguez, A generalization of the adaptive rejection sampling algorithm, *Stat. Comput.* **21**, 633 (2011).
- [38] S. G. Nurzaman, Y. Matsumoto, Y. Nakamura, K. Shirai, S. Koizumi, and H. Ishiguro, From Lévy to Brownian: A computational model based on biological fluctuation, *PLoS One* **6**, e16168 (2011).
- [39] M. R. Shaebani and H. Rieger, Transient anomalous diffusion in run-and-tumble dynamics, *Front. Phys.* **7**, 120 (2019).
- [40] S. Engblom, P. Lötstedt, and L. Meinecke, Mesoscopic modeling of random walk and reactions in crowded media, *Phys. Rev. E* **98**, 033304 (2018).



- [41] T. Kaya and H. Koser, Direct upstream motility in *Escherichia coli*, *Biophys. J.* **102**, 1514 (2012).
- [42] J. Taktikos, V. Zaboradaev, and H. Stark, Collective dynamics of model microorganisms with chemotactic signaling, *Phys. Rev. E* **85**, 051901 (2012).
- [43] L. Turner, W. S. Ryu, and H. C. Berg, Real-time imaging of fluorescent flagellar filaments, *J. Bacteriol.* **182**, 2793 (2000).
- [44] L. Cisneros, C. Dombrowski, R. E. Goldstein, and J. O. Kessler, Reversal of bacterial locomotion at an obstacle, *Phys. Rev. E* **73**, 030901(R) (2006).
- [45] S. Bianchi, F. Saglimbeni, A. Lepore, and R. Di Leonardo, Polar features in the flagellar propulsion of *E. coli* bacteria, *Phys. Rev. E* **91**, 062705 (2015).
- [46] G. J. McLachlan and D. Peel, *Finite Mixture Models* (John Wiley & Sons, New York, 2004).
- [47] K. Taute, S. Gude, S. Tans, and T. Shimizu, High-throughput 3D tracking of bacteria on a standard phase contrast microscope, *Nat. Commun.* **6**, 8776 (2015).
- [48] P. L. Irwin, L.-H. T. Nguyen, G. C. Paoli, and C.-Y. Chen, Evidence for a bimodal distribution of *Escherichia coli* doubling times below a threshold initial cell concentration, *BMC Microbiol.* **10**, 207 (2010).
- [49] K. J. Duffy, P. T. Cummings, and R. M. Ford, Random walk calculations for bacterial migration in porous media, *Biophys. J.* **68**, 800 (1995).
- [50] K. J. Duffy and R. M. Ford, Turn angle and run time distributions characterize swimming behavior for *Pseudomonas putida*, *J. Bacteriol.* **179**, 1428 (1997).
- [51] A. Creppy, E. Clément, C. Douarche, M. V. D'Angelo, and H. Auradou, Effect of motility on the transport of bacteria populations through a porous medium, *Phys. Rev. Fluids* **4**, 013102 (2019).
- [52] E. M. Calvo-Muñoz, M. E. Selvan, R. Xiong, M. Ojha, D. J. Keffer, D. M. Nicholson, and T. Egami, Applications of a general random-walk theory for confined diffusion, *Phys. Rev. E* **83**, 011120 (2011).
- [53] S. C. Weber, M. A. Thompson, W. E. Moerner, A. J. Spakowitz, and J. A. Theriot, Analytical tools to distinguish the effects of localization error, confinement, and medium elasticity on the velocity autocorrelation function, *Biophys. J.* **102**, 2443 (2012).
- [54] R. Metzler, J.-H. Jeon, and A. Cherstvy, Non-Brownian diffusion in lipid membranes: Experiments and simulations, *Biochim. Biophys. Acta Biomembr.* **1858**, 2451 (2016).
- [55] M. A. Desposito and A. D. Viales, Subdiffusive behavior in a trapping potential: Mean square displacement and velocity autocorrelation function, *Phys. Rev. E* **80**, 021111 (2009).
- [56] M. Weiss, M. Elsner, F. Kartberg, and T. Nilsson, Anomalous subdiffusion is a measure for cytoplasmic crowding in living cells, *Biophys. J.* **87**, 3518 (2004).